Heliyon 10 (2024) e32135

Contents lists available at ScienceDirect

Heliyon

journal homepage: www.cell.com/heliyon

Research article

In situ forming an injectable hyaluronic acid hydrogel for drug delivery and synergistic tumor therapy

Sisi Fan [a,b,1], Qinghuan Liu [a,b,1], Jia Dong [a,b], Xiaorui Ai [a,b], Jing Li [a,b,*], Wei Huang [a,b,**], Taolei Sun [a,b,c,***]

[a] School of Chemistry, Chemical Engineering and Life Science, Wuhan University of Technology, Wuhan, 430070, China
[b] Hubei Key Laboratory of Nanomedicine for Neurodegenerative Diseases, School of Chemistry, Chemical Engineering and Life Science, Wuhan University of Technology, 122 Luoshi Road, Wuhan, 430070, China
[c] State Key Laboratory of Advanced Technology for Materials Synthesis and Processing, Wuhan University of Technology, 122 Luoshi Road, Wuhan, 430070, China

ARTICLE INFO

Keywords:
Hyaluronic acid hydrogel
Localized injectability
Stimulus-responsive
Drug delivery system
Synergistic therapy

ABSTRACT

Stimulus-responsive injectable hydrogel has the key characteristics of in situ drug-loading ability and the controlled drug release, enabling efficient delivery and precise release of chemotherapy drugs at the tumor site, thereby being used as a local drug delivery system for sustained tumor treatment. This article designed a smart responsive injectable hydrogel loaded with anti-tumor drugs and nanoparticles to achieve efficient and specific synergistic treatment of tumors. Hyaluronic acid (HA) hydrogel obtained by cross-linking HA-SH (HS) and HA-Tyr (HT) through horseradish peroxidase (HRP), and doxorubicin hydrochloride (DOX) and folic acid-polyethylene glycol-amine (FA-PEG-NH_2) modified PDA (denoted as PPF) were encapsulated to construct the HS/HT@PPF/D hydrogel. The hydrogel had good biocompatibility, injectability, and could respond to multiple stimuli at the tumor site, thereby achieving controlled drug release. At the same time, PPF gave it excellent photothermal efficiency, photothermal stability and tumor targeting. In vitro and in vivo experimental results showed that the HS/HT@PPF/D hydrogel combined with near-infrared laser irradiation could significantly improve its anti-tumor effect and could almost eliminate the entire tumor mass without obvious adverse reactions. The HS/HT@PPF/D hydrogel could achieve multi-stimulus-responsive drug delivery and be used for precise chemo-photothermal synergistic tumor treatment, thus providing a new platform for local synergistic tumor treatment.

1. Introduction

Cancer poses a significant threat to human health and has emerged as a leading cause of mortality [1]. In recent years, localized chemotherapy has garnered increasing attention as a viable approach in cancer treatment, particularly for treating superficial solid

* Corresponding author.
** Corresponding author.
*** Corresponding author.
E-mail addresses: lij@whut.edu.cn (J. Li), huangwei2020@whut.edu.cn (W. Huang), suntl@whut.edu.cn (T. Sun).
[1] These authors contributed equally to this work.

https://doi.org/10.1016/j.heliyon.2024.e32135
Received 25 February 2024; Received in revised form 24 May 2024; Accepted 28 May 2024
Available online 29 May 2024

tumors accessible to local intervention methods [2]. Compared with intravenous injection, local chemotherapy increases the bioavailability of drugs at the tumor site and reduces their adverse systemic effects [3]. However, the necessity for repetitive drug injections in localized therapy often results in poor patient compliance [4]. Hence, there arises a pressing need to develop drug carriers capable of targeted and sustained delivery, facilitating gradual drug release directly into tumors and reducing the frequency of administrations.

Hydrogels have attracted widespread attention in the biomedical field due to their low invasiveness, high drug bioavailability, sustained drug release, low systemic toxicity and high capacity of drug loading [5–9]. As ideal drug delivery carriers, the hydrogels from the natural polymers and synthetic polymers with good biocompatibility and no-immunostimulatory activity are biodegradable [10–13].

Natural polysaccharides have received significant attention for applications of biomedical carrier materials (e.g., hyaluronic acid (HA), sodium alginate, chitosan, cellulose and gelatin) due to multiple functional groups modified in various ways to change characteristics [14–18]. The chemical modification of functional groups is the key issue to control the structural properties of hydrogel, including stability, mechanical properties and biodegradation [19]. The modification methods of polysaccharides mainly include sulfation, carboxymethylation, acetylation, etc. [20] In addition, stimulus responsiveness also plays a key role in the controlled release of drugs. Ordinary hydrogels can release drugs slowly, but the speed and dosage of drug release are uncontrollable [21]. In contrast, stimuli-responsive hydrogels can be loaded with drugs to achieve controllable release of drugs under endogenous microenvironmental stimulation (such as mildly acidic pH, hypoxia, high glutathione (GSH) and overexpression of specific enzymes) or exogenous physical stimulation (e.g., light, temperature, magnetism and ultrasound) [22–26]. In particular, disulfide bonds have been extensively explored for the development of redox-responsive hydrogels [27]. Because the intracellular glutathione levels of tumor cells are several times higher than that of normal cells [28]. When redox hydrogels loaded with therapeutic agents enter the tumor cells, they will be degraded by the high concentration of glutathione [29]. According to those studies, multiple response hydrogels have been developed [30–32]. In particular, stimuli-responsive in situ injected hydrogels formed can be widely used for superficial malignant tumors, such as melanoma and breast cancer [33]. One single peritumoral administration can achieve high inhibition efficacy against tumor recurrence [34].

However, considering the multi-layered complexity of tumors, single-modality treatment strategies are far from satisfactory, and simple drug delivery hydrogels may still not meet anti-cancer requirements. The combination of chemotherapy and other treatments is

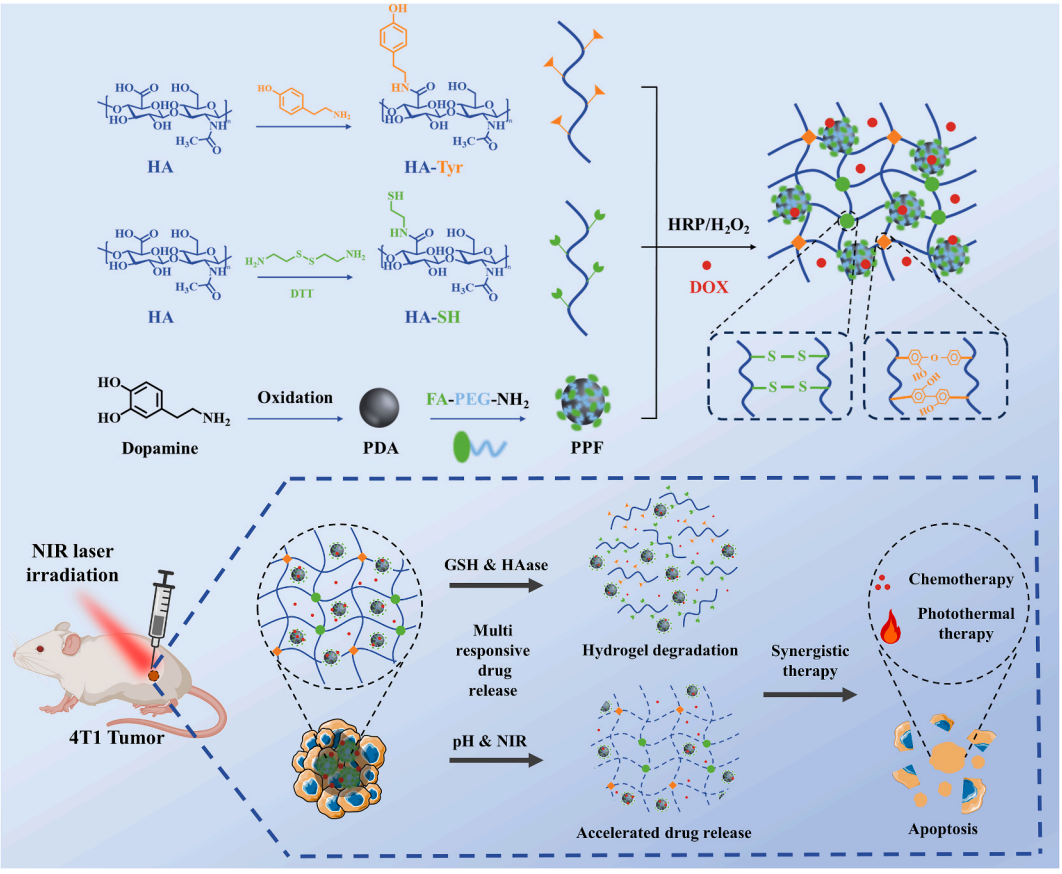

Fig. 1. Schematic illustration of the HS/HT@PPF/D hydrogel preparation and chemo-photothermal synergistic therapies of tumors.

considered a promising cancer treatment method, such as chemotherapy combined with photothermal therapy, photodynamic therapy, immunotherapy, etc. [35–38] Photothermal therapy (PTT) represents a non-invasive approach to cancer treatment, utilizing photothermal materials with strong absorption in the near-infrared (NIR) spectrum to convert light energy into heat energy, thereby facilitating local ablation of deep-seated tumors [39,40]. In recent years, polydopamine nanoparticles (PDA) have emerged as promising candidates due to their exceptional photothermal conversion efficiency, biocompatibility and biodegradability. PDA not only serves as an effective photothermal agent for cancer cell ablation via PTT but also functions as a versatile nanocarrier for triggered drug release upon NIR laser irradiation [41,42]. In addition, PTT has been shown to enhance the sensitivity of tumor cells to chemotherapy drugs, enabling synergistic chemo-photothermal treatment [43].

This work constructed HA hydrogels loaded with folic acid-polyethylene glycol-amine (FA-PEG-NH_2) modified PDA nanoparticles (denoted as PPF) and the anti-tumor drug doxorubicin hydrochloride (DOX), termed as HS/HT@PPF/D hydrogel for chemo-photothermal synergistic therapy in tumor treatment (Fig. 1). Using sulfhydryl-modified HA (HS) and tyramine-modified HA (HT), we formulated an injectable HA hydrogel that forms in situ by enzymatic cross-linking, involving disulfide bond formation and phenol-phenol cross-linking. The hydrogel exhibited specific responsiveness to various stimuli within the tumor microenvironment (TME), facilitating the targeted delivery of anti-tumor drugs to tumor cells. This sustained local drug release maintained optimal drug concentrations at the tumor site, thereby enhancing therapeutic agent bioavailability and efficacy, while minimizing systemic toxicity and side effects. Under the irradiation of NIR laser, the hydrogel loaded with PPF and DOX rapidly heated to temperatures exceeding 60 °C, enabling effective photothermal ablation of tumor cells. Furthermore, that also accelerate the release of DOX to enhance drug accumulation and penetration within tumors. Our findings demonstrate that the responsive injectable HS/HT@PPF/D hydrogel prepared based on enzymatic cross-linking effectively inhibited tumor growth both in vitro and in vivo. This system represents a promising local drug delivery for tumor treatment.

2. Materials and methods

2.1. Materials

Hyaluronic acid (HA, MW 100–200 kDa) was obtained from Macklin Biochemical Co. (Shanghai, China). Dopamine hydrochloride, tyramine hydrochloride, DOX, DL-dithiothreitol (DTT), 1-Ethyl-3-(3-dimethylaminopropyl) carbodiimide hydrochloride (EDC), *N*-hydroxysulfosuccinimide (NHS, 98 %), FA-PEG-NH_2 (MW 2000 Da), cystamine dihydrochloride, tris-hydrochloric acid buffer solution, horseradish peroxidase (HRP, RZ $\geq$ 3.0) and hydrogen peroxide (H_2O_2, 30 %) were purchased from Aladdin (Shanghai, China).

2.2. Synthesis of HA-tyr and HA-SH

HA-SH (HS) was prepared through a two-step reaction. Firstly, HA (1.0 g) was dissolved in distilled water (50 mL), then mixed with EDC (1.915 g) and NHS (1.15 g), adjusted to pH 5.0, and stirred at room temperature for 1 h. Cystamine dihydrochloride (1.69 g) was then added to continue the reaction for 24 h to modify the HA, and the product was dialyzed with deionized water for 1 d for later use. Subsequently, the pH of the above solution was adjusted to 8–8.5 with 1 M NaOH, then DTT (2.313 g) was added to the mixture, and the reaction was continued for 24 h under N_2 to cleave the disulfide bond. This was followed by dialysis in dilute HCl (pH 5.0) containing 5 g L^{-1} NaCl, dilute HCl (pH 5.0) for 3 d, and finally the dialysate was lyophilized to obtain HS.

HA-Tyr (HT) was synthesized by coupling tyramine hydrochloride to the HA via an EDC/NHS-mediated carbodiimide coupling reaction. HA (1.0 g) was mixed with EDC (1.915 g) and NHS (1.15 g), adjusted the pH of the solution to 5.0, and stirred at room temperature for 1 h. Tyramine hydrochloride (1.31 g) was added and the reaction continued for 24 h, followed by dialyzed against 100 mM NaCl for 1 d and then against deionized water for 2 d. Finally, the dialysate was lyophilized to obtain HT.

2.3. Synthesis of PPF

Ammonia aqueous solution (28–30 %, 4 mL), ethanol (30 mL) and deionized water (70 mL) were mixed under mildly magnetic stirring at room temperature. Dopamine hydrochloride (0.5 g) was added to the above solution and reacted for 24 h, then centrifuged (10,000 rpm, 15 min) and washed to obtain PDA. In order to improve the targeting of nanoparticles, PDA and FA-PEG-NH_2 were stirred vigorously in Tris-HCl buffer for 12 h, and then PPF was obtained by centrifugation [44].

2.4. In situ hydrogel formation and gelation time determination

HS solution (480 μL) and HRP solution (20 μL) were added to a tube (solution A). In another tube, HT solution (480 μL) was mixed with H_2O_2 (20 μL; solution B). Solution A and B were mixed to form HS/HT hydrogel. Similarly, for the synthesis of HS/HT@PPF/D hydrogel, HT solution (480 μL) containing well-mixed PPF and DOX solution was mixed with H_2O_2, then mixed with HS and HRP (Fig. 1). The gelation time was determined using an inverted tube test every 30 s.

2.5. Morphological study

The internal morphologies of the hydrogels were characterized by scanning electron microscopy (SEM, Zeiss Ultra Plus) after lyophilizing, breakage, and gold spraying.

2.6. Rheological behavior of hydrogels

A Kinexus Ultra + rheometer was used for rheological performance testing of the hydrogels. The storage modulus (G′) and loss modulus (G″) of the hydrogel were recorded by changing strain scanning (0.1–500 %, frequency fixed at 1 Hz) at a test temperature of 37 °C.

2.7. Degradation behavior in vitro

To determine the degradation behavior of the hydrogels, the lyophilized hydrogels were placed in different buffer mediums at 37 °C and the quality of hydrogels before and after degradation were compared. The percent degradation of the hydrogel was calculated according to the formula:

$$\text{Degradation} = \frac{(W_o - W_d)}{W_o} \times 100\% \quad (1)$$

where W_o is the initial dry weight of the hydrogel and W_d is the dry weight of the hydrogel after degradation.

2.8. Stimulus-responsive DOX release

Drug-loaded hydrogels were transferred into the dialysis bag and dialyzed under different buffer media (pH 5.0, 7.4, 7.4 + 10 μM GSH, 5.0 + 10 mM GSH, 7.4 + 50 U mL^{-1} hyaluronidase (HAase), 5.0 + 50 U mL^{-1} HAase) or 808 nm NIR laser irradiation (2 W cm^{-2}, 10 min). Due to the stimuli-responsive of the HS/HT@PPF/D hydrogel, DOX could be released from the hydrogel and diffused out of the dialysis bag into the external PBS solution. At specific time intervals, 3 mL supernatant was removed for testing by the UV–Vis spectrophotometry at 480 nm according to the standard curve of drugs, simultaneously an equal volume of corresponding buffer media was supplemented.

2.9. Photothermal performance

HS/HT@PPF/D hydrogels with PPF concentrations of 0.1, 0.2, 0.5 and 1.0 mg mL^{-1} respectively were irradiated with an 808 nm laser at different powers for 10 min. The temperature of the solution and hydrogel were measured every 30 s. We selected 0.5 mg mL^{-1} PPF for the following experiments. Record the temperature curve of PPF irradiated with an 808 nm laser at 2.0 W cm^{-2} for 10 min, then naturally cool down, and calculate the photothermal conversion efficiency of PPF. In order to test the stability of HS/HT@PPF/D hydrogel, the experiment was repeated 4 times in a row.

2.10. Hemolysis test

To assess the hemocompatibility of hydrogels in vitro, the hemolysis test was performed. Blood samples from the Balb/c mice were collected with anticoagulant and centrifuged at 2000 rpm for 10 min to obtain the red blood cells (RBC). In brief, 1.0 mL RBC suspension was incubated with 2.0 mg different hydrogels, respectively. Meanwhile, the PBS buffer and water were used as the negative and positive controls. After incubated at 37 °C for 5 h, the RBC were centrifuged for 10 min with 2000 rpm to obtain the supernatant and measure its absorbance at 541 nm. Calculate the hemolysis rate according to the formula:

$$HR = \frac{(OD_t - OD_n)}{OD_p - OD_n} \times 100\% \quad (2)$$

where HR is the hemolysis rate, OD_t is the absorbance of the experimental group, OD_p is the absorbance of the positive control group, and OD_n is the absorbance of the negative control group.

2.11. In vitro cell uptake and cytotoxicity assay

Murine fibroblasts cells (L929) and murine breast cancer cells (4T1) were obtained from the School of Chemistry, Chemical Engineering, and Life Science, Wuhan University of Technology, Wuhan, China. L929 cells and 4T1 cells were seeded and cultured for 24 h separately. The cells were co-incubated with free DOX or DOX-loaded PPF for 2 h, then dyed with DAPI and observed under an inverted fluorescence microscope.

CCK-8 assay was used to evaluate the cytotoxicity of different hydrogels and different concentration of PPF in L929 cells. Briefly, L929 cells were cultured in the lower chamber of the transwell plate and incubated for 24 h. Then sterilized hydrogels were added to the upper compartment. After continuing to culture for 24 h, added CCK-8 to the well plate, and placed it in a 37 °C incubator for 2 h. Used a multifunctional microplate reader to measure the absorbance at a wavelength of 450 nm. To evaluate the chemo-photothermal synergistic effects, 4T1 cells were treated with sterilized hydrogels with or without NIR laser irradiation. Similarly, after continuing to culture for 24 h, added CCK-8 to the well plate, and placed it in a 37 °C incubator for 2 h. Used a multifunctional microplate reader to measure the absorbance at a wavelength of 450 nm.

In addition, the L929 and 4T1 cells were treated with the same groups of samples for 24 h, and then Hoechst 33342/PI staining was

performed to observe live and dead cells. Hoechst staining solution and PI staining solution in proportion and stained at 4 °C for 20 min. After staining, rinsed gently with PBS solution, and then placed the cells under the inverted fluorescence microscope for observation.

2.12. In vivo anticancer therapy

All animal procedures were approved by the Experimental Animal Ethics Committee of Wuhan University of Technology and complied with all relevant ethical regulation (WHUT.2023–006). Balb/c mice (female, 5-week-old) were purchased from Hubei Experimental Animal Research Center. The tumor model was established by injecting 4T1 cells (2.0×10^6 per mouse) into the back of mice and then the mice were monitored by checking the tumor volume daily until it reached around 100 mm^3. Subsequently, these mice were divided into seven groups (5 mice/group) with various treatments including PBS, PBS + Laser, DOX, HS/HT@PPF hydrogel, HS/HT@PPF/D hydrogel, HS/HT@PPF hydrogel + Laser and HS/HT@PPF/D hydrogel + Laser. 50 μL of solution were injected to each mouse. NIR laser was irradiated at 1.0 W cm^{-2} for 5 min for each treatment. After treatments, tumor volume and body weight of mice were recorded every two days. The mice were euthanized at day 12. Immediately, the tumor and the major organs (heart, liver, lung, spleen and kidney) were removed, washed, photographed, and then sectioned for H&E and TUNEL staining.

2.13. Statistical analysis

Data were calculated mean ± standard deviation (SD) precisely and the statistical significance between groups in the experiments was analyzed based on student's t-test and one-way ANOVA. *$p < 0.05$, **$p < 0.01$, ***$p < 0.001$.

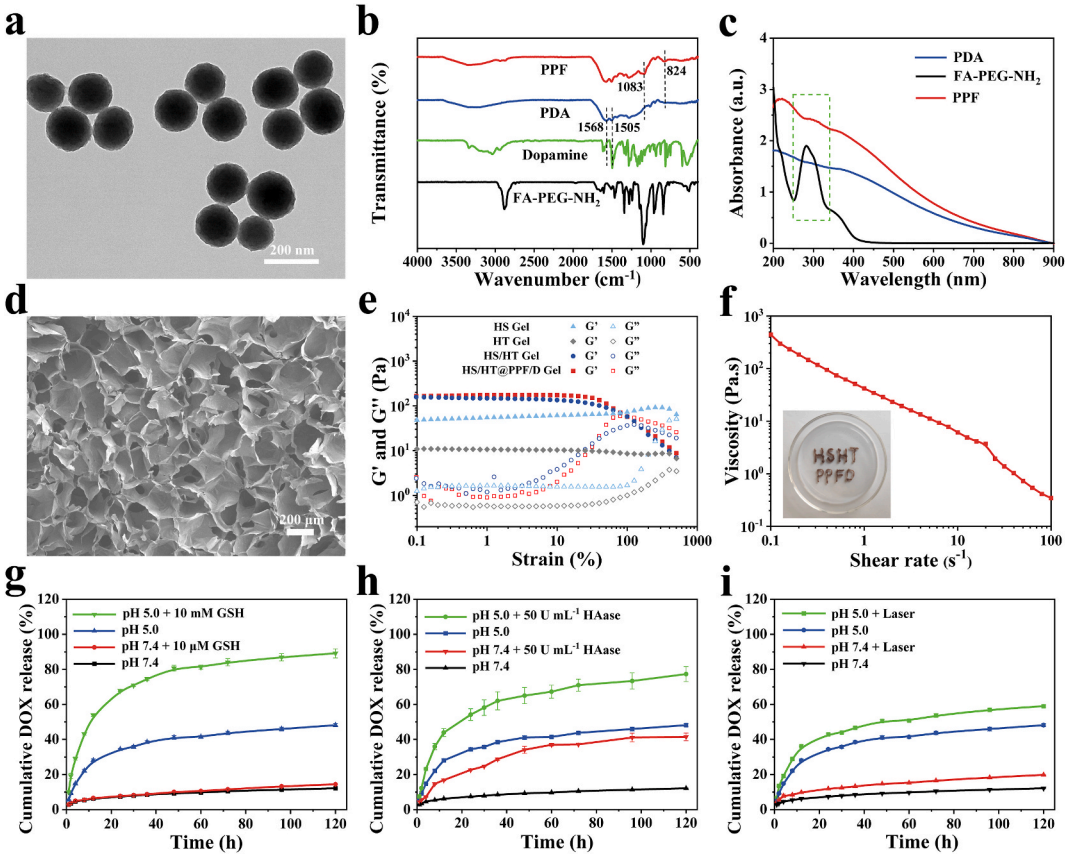

Fig. 2. (a) TEM image of PPF. (b) FT-IR spectra and (c) UV–Vis absorption spectra of PDA and PPF. (d) SEM images of HS/HT@PPF/D hydrogel. (e) Rheological properties of HS hydrogel, HT hydrogel, HS/HT hydrogel and HS/HT@PPF/D hydrogel (G′, storage modulus and G″, loss modulus). (f) Shear thinning behavior and the injectable behavior of HS/HT@PPF/D hydrogel. In vitro DOX release behavior of HS/HT@PPF/D hydrogel in PBS, pH 7.4 and 5, with or without (g) GSH, (h) HAase and (i) 808 nm NIR laser (2 W cm^{-1}, 10 min).

3. Results and discussion

3.1. Preparation and characterization of HS/HT@PPF/D hydrogel

The synthetic scheme of HS, HT, PPF, and HS/HT@PPF/D hydrogels were presented in Fig. 1. The HS/HT@PPF/D hydrogel was dual-crosslinked via the thiol groups of HS and the phenol functional group of HT. The structures of HS and HT were characterized through ^{1}H NMR, FT-IR spectra and UV–Vis absorption spectra. As shown in the spectra (Fig. S1a), the intensity of the in-plane bending vibration peak of the amide II band –NH at 1560 cm^{-1} was significantly enhanced, indicating the formation of new amide bonds after the reaction of HA and cystamine dihydrochloride. The absorption peaks at $\delta = 2.4$ ppm and $\delta = 2.6$ ppm were the proton absorption peaks of the two methylene groups on the cysteamine group, further proving that HS was successfully synthesized (Fig. S1b). The UV–Vis absorption spectra showed that HT has an obvious benzene ring absorption peak at 275 nm (Fig. S1c). In addition, the absorption peaks at $\delta = 6.8$ ppm and $\delta = 7.1$ ppm in ^{1}H NMR spectrum were the proton absorption peaks on the tyramine benzene ring (Fig. S1d). The UV–Vis spectra and ^{1}H NMR proved that HT was successfully synthesized.

The addition of PPF in hydrogels provided a condition for PTT. PDA was self-polymerized by the oxidation of dopamine under alkaline condition, and are modified by FA-PEG-NH_2 to obtain PPF to improve its active targeting [44–46]. According to TEM results (Fig. 2a and Figs. S2a–c), PDA and PPF were uniformly dispersed spherical structures, and the average diameters of PDA and PPF were both about 147 nm. The DLS results (Fig. S2d) showed that the hydrodynamic diameters of PDA and PPF were 149.3 nm and 220.5 nm, respectively. An increase in hydrodynamic diameter after FA-PEG-NH_2 modification may be attributed to the presence of the outer polymer layer of PDA. The zeta potential of PDA was −37.2 mV due to the contribution of phenolic hydroxyl groups, and after modification of FA-PEG-NH_2, the surface zeta potential of PPF increased to −26.7 mV (Fig. S2e). In addition, the particle size of PPF remained basically unchanged within two weeks indicating that PPF can maintain stable for a long time (Fig. S2f). The chemical modification of PDA was verified via FT-IR and UV–Vis spectra. From the FT-IR spectra of PDA (Fig. 2b), peaks at 3600-3000 cm^{-1} could be ascribed to the stretching vibration of –NH and –OH, while those at 1568 and 1505 cm^{-1} results from the aromatic C═C bond of indole. The peaks of –CH_2-CH_2-*O*- and = CH at 1083 cm^{-1} and 824 cm^{-1} represents the characteristic peaks of PPF. Those results demonstrated the synthesis of PDA and the successful grafting of FA-PEG-NH_2. From the UV–Vis spectrum (Fig. 2c), it could be found that both PDA and PPF had broad absorption from the ultraviolet to NIR band. PPF had an absorption peak at 283 nm, which was resulted from the π-π* transition of the pterin ring in FA, further confirming the successful synthesis of PPF.

HS, HT, HS/HT and HS/HT@PPF/D hydrogels were formed through enzymatic crosslinking via the sulfhydryl group of HS and the phenol group of HT [47,48]. As shown in Fig. S3, the water content of the hydrogels exceeded 98 %, and the internal morphology of the hydrogels was studied using SEM (Fig. 2d and Fig. S4). The internal structure of the hydrogels was porous, showing an interconnected network structure. PPF nanoparticles could clearly be observed attached to the hydrogel surface in the HS/HT@PPF/D hydrogel (Fig. S5). Controllable gelation time and injectability of hydrogels were very important for local treatment of tumors. The vial-inversion method was using to determine the gelation time. At constant concentrations of HRP and H_2O_2, the HS concentration was increased from 0.5 % to 2 %, and the gelation time was reduced from approximately 3 h to 23 min (Fig. S6a). In addition, with increasing the HT concentration from 0.25 % to 2 % the gelation time was shortened from about 5 min to 30 s (Fig. S6b). From a practical applications point of view, too fast gelation may lead to the hydrogel to be uneven or lead to needle clogging during injection. But slow gelation may cause the hydrogel precursor solution injected into the body to be diluted and washed away by tissue fluid, making it impossible to fix and maintain the loaded drug [35]. The gelation time of HS hydrogel was long, which was not conducive to the formation of hydrogel in situ. However, the presence of phenolic substances could promote the enzyme-catalyzed thiol oxidation to induce the formation of disulfides, when phenol-phenol cross-links were formed under enzyme catalysis [48]. Furthermore, when the concentrations of HS, HT, HRP and H_2O_2 were all fixed, the addition of PPF had little effect on the gelation rate (Fig. S6c). By adjusting the concentration of each component with the HS/HT@PPF/D hydrogel (2.0 wt% HS and 0.5 wt% HT), the gelation time of the hydrogel could be controlled within 2–4 min.

In addition to gelation time, the mechanical properties of hydrogels will limit the biomedical. A rotational rheometer was used to further evaluate the mechanical properties of the hydrogels (Fig. 2e). In the oscillatory strain scanning test, the HS/HT@PPF/D hydrogels had a greater G′ (storage modulus) than G'' (loss modulus) within the strain limit range, from 0.1 % to 100 %, indicating that it had elastic properties. When the yield strain was greater than 100 %, the intersection of the G′ and G″ curves appeared, indicating that the yield strain had flow characteristics (G″ > G′) rather than solid characteristics. Moreover, the shear thinning performance of the hydrogel confirmed the injectable property of the hydrogel (Fig. 2f). At the same time, ''HSHTPPFD'' could be quickly injected through a syringe, indicating that HS/HT@PPF/D hydrogel had excellent injectability.

To measure the stability and stimulated degradation of hydrogel, weight loss in vitro and biodegradation in vivo were evaluated. The results showed that the weight of HS/HT@PPF/D hydrogel was relatively stable under normal physiological conditions, while hydrogels could be rapidly degraded in TME such as HAase and reducing conditions (Fig. S7a). Furthermore, to evaluate the gelation and degradation of the hydrogel in vivo, the hydrogel was injected subcutaneously into the right back of the mice. The HS/HT@PPF/D hydrogel could be formed in situ within 30 min, which showed a slight bulge (Fig. S7b). In addition, with implantation time of the hydrogel increasing, the volume and mass of the hydrogel gradually decreased (Fig. S7c). The results showed that HS/HT@PPF/D hydrogel had the ability of in-situ formation and controllable degradation, which ensured the biosafety of the HS/HT@PPF/D hydrogel. The hydrogel was expected to serve as carrier materials for topical therapeutic delivery of drugs. The biosafety of HS/HT@PPF hydrogel was further evaluated by blood biochemical indexes in mice. The results showed that there was no significant difference in the HS/HT@PPF treatment group compared with the control (Fig. S8). This indicated that HS/HT@PPF hydrogel had good biocompatibility.

To assess the drug release behavior of hydrogels encapsulating DOX, the drug release was evaluated in buffer media (pH 5.0 and pH 7.4) under different environments. Due to the reduction and enzyme response properties of the HS/HT@PPF/D hydrogel, we selected release media with different concentrations of GSH and HAase to simulate normal and tumor environments. When the pH value lowered from 7.4 to 5.0, the cumulative release rate increased from 12.12 % to 48.16 % at 120 h. Furthermore, the release rate increased to 89.20 % with the addition of GSH (10 mM) at pH 5.0 for 120 h incubation time (Fig. 2g). The factor of HAase (50 U mL^{-1}) also accelerated the release rate of DOX by approximately 30 % (Fig. 2h). The results demonstrated that the factor of environment pH, GSH and HAase could effectively trigger the selective release of DOX in the HS/HT@PPF/D hydrogel. Moreover, as illustrated in Fig. 2i, the group with laser had a significantly higher cumulative release of DOX compared to the group without laser, suggesting that photothermal effect could enhance the release of DOX from the hydrogel. These results indicated the HS/HT@PPF/D hydrogel could be controlled by endogenous lower pH, reduction environment, HAase and exogenous NIR irradiation-responsive release to minimize the side effects.

3.2. Photothermal performance

Tumor cells are more sensitive to heat in comparison to non-diseased cells, and high temperature exposure results in tumor cells more susceptible to chemotherapy or radiation therapy. To assess the efficacy of photothermal agent of PPF and the photothermal efficiency of HS/HT@PPF/D hydrogel, the temperature variation was recorded by infrared imaging. As shown in Fig. 3a, the temperature change of HS/HT@PPF/D hydrogel can be controlled by adjusting the concentration of PPF (0–1.0 mg mL^{-1}). The temperature variation curves of the HS/HT@PPF/D hydrogel with PPF (0.5 mg mL^{-1}) under different laser powers (0.5–2.5 W cm^{-2}) showed that the temperature can be adjusted by laser power (Fig. 3b). The temperatures of PPF solution (0.5 mg mL^{-1}) and HS/HT@PPF/D hydrogel (0.5 mg mL^{-1} PPF) could increase to 65.3 °C and 69.0 °C under irradiation with an 808 nm laser at a density of 2.0 W cm^{-2} for 10 min. The treatment temperature was easily maintained above 43 °C, which is considered to be a temperature that can kill tumor cells. In contrast, HS/HT hydrogel only showed a slight temperature increase, confirming that the photothermal performance of the HS/HT@PPF/D hydrogel originated from PPF (Fig. 3c). From the cycles of four consecutive heating and cooling experiments, HS/HT@PPF/D hydrogel could be heated and cooled stably, indicating that the hydrogel had stable photothermal conversion capability (Fig. 3d and f). The photothermal conversion efficiency of PPF was also calculated to be approximately 38.81 % by Roper's method (Fig. 3e) [49]. The good photothermal effect and stable photothermal conversion ability of HS/HT@PPF/D hydrogel demonstrated the hydrogel was a durable photothermal agent, that can be used for repeated photothermal treatment of tumors.

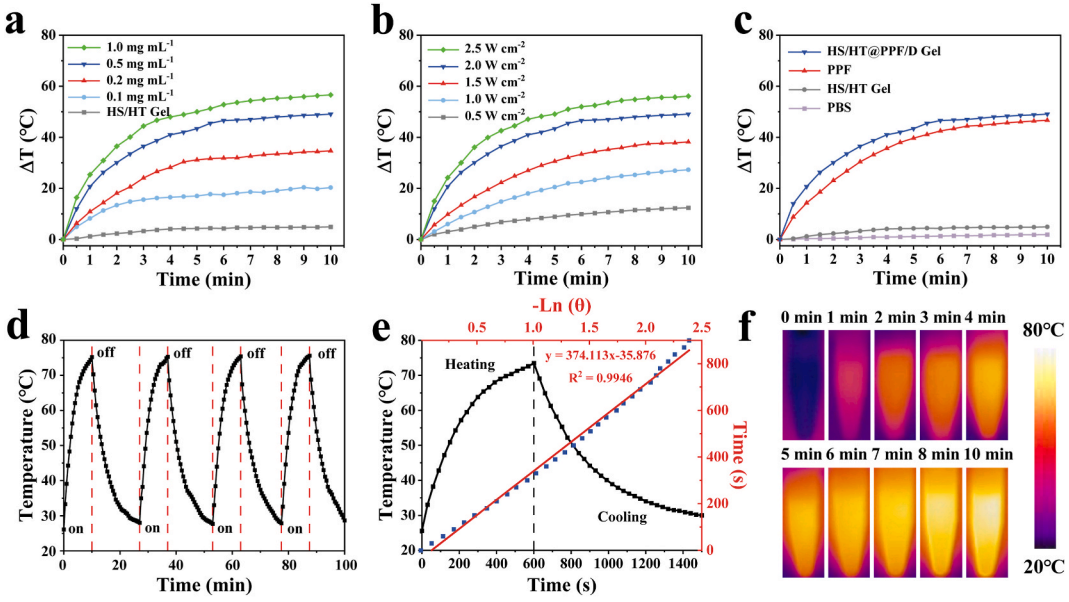

Fig. 3. The temperature change of (a) HS/HT@PPF/D hydrogel exposed to 808 nm, 2.0 W cm^{-2} laser for 10 min with different concentrations of PPF. (b) The temperature change of HS/HT@PPF/D hydrogel (0.5 mg mL^{-1} PPF) exposed to 808 nm laser for 10 min with different powers. (c) Temperature changes of HS/HT@PPF/D hydrogel, PPF, HS/HT hydrogel and PBS exposed to 808 nm laser for 10 min. (d) Temperature change of HS/HT@PPF/D hydrogel exposed to 808 nm laser intermittently for 100 min. (e) Photothermal conversion efficiency of PPF. (f) Photothermal images of HS/HT@PPF/D hydrogel (0.5 mg mL^{-1} PPF) exposed to 808 nm, 2.0 W cm^{-2} laser for 10 min.

3.3. Cytotoxicity, anti-tumor efficacy and cellular uptake in vitro

To assess the biocompatibility of the HS/HT@PPF/D hydrogel drug delivery system, the cytotoxicity of its individual components on L929 cells using the CCK-8 assay. When L929 cells were incubated with HS, HT, HS/HT, HS/HT@PPF hydrogel, PDA and PPF for 24 h, the cell viability reached over 85 %, which showed that the construction material of drug delivery systems had good biocompatibility (Fig. 4a–b). The live/dead cell staining using Hoechst 33342/PI also showed that the HS/HT@PPF hydrogel had good biocompatibility (Fig. S9). In addition, we also explored the hemolysis activity of each component of the HS/HT@PPF/D hydrogel (Fig. S10). Each component of the HS/HT@PPF/D hydrogel did not cause obvious hemolysis as the negative control group, further indicating that the hydrogel had good blood compatibility.

Furthermore, we evaluated the anti-tumor effect of the HS/HT@PPF/D hydrogel on 4T1 cells. As shown in Fig. 4c, the cell viability of HS/HT@PPF/D hydrogel was 77.02 % compared with DOX group (40.00 %) without laser, which was attributed to the sustained release effect of HS/HT@PPF/D hydrogel. Compared with the HS/HT@PPF/D hydrogel group (77.02 %) and HS/HT@PPF hydrogel + Laser group (24.60 %), the chemotherapy drugs of DOX and photothermal therapy of PPF decreased cell viability to 9.78 % in the HS/HT@PPF/D hydrogel + Laser group. In addition, the results of Hoechst 33342/PI (Fig. 4d) also confirmed that the HS/HT@PPF/D hydrogel with laser irradiation group exhibited the best anti-tumor activity, which was consistent with the results of CCK-8. These results showed that HS/HT@PPF/D hydrogel has significant synergistic chemotherapy and phototherapy effect of tumor.

To assess the active targeting ability of DOX-loaded PPF nanoparticles, the uptake behavior of nanoparticles was determined using 4T1 cells overexpressing folate receptor (FR) and L929 cells with low FR expression (Fig. 4e–f). The cells treated with DOX had no significant fluorescence change because free DOX had no specific recognition of L929 cells and 4T1 cells. Nonspecific cellular internalization could cause severe toxic side effects in normal cells. However, the fluorescence intensity of 4T1 cells group incubated with PPF/D was significantly stronger than that of L929 cells group, indicating that PPF/D could be specifically taken up by cancer cells. The

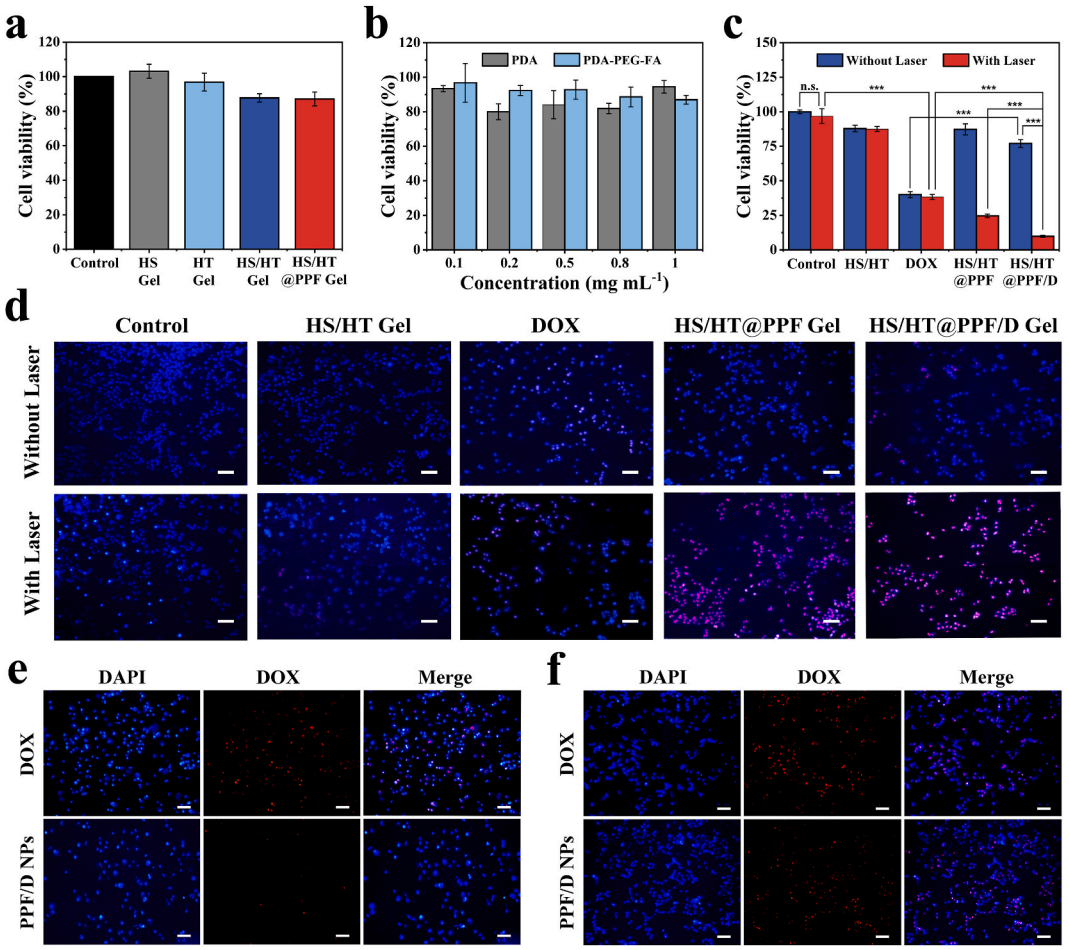

Fig. 4. Cytotoxicity of (a) Hydrogels, (b) PDA and PPF and (c) Hydrogels with or without 808 nm laser. (d) Live/dead staining assay of hydrogels with or without 808 nm laser, blue fluorescence for live cells and red fluorescence for dead cells. (e) L929 cells and (f) 4T1 cells after incubation with free DOX and DOX-loaded PPF for 2 h. Scale bar: 200 μm. (Student's t-test, n = 3, n.s., no significance, ***p < 0.001). (For interpretation of the references to colour in this figure legend, the reader is referred to the Web version of this article.)

uptake ratio increased from 4.7 % to 75.8 % (Fig. S11). PPF/D had excellent ability to target tumor cells and reduce the endocytosis of normal cells, reducing the toxic side effects of drugs on normal cells.

3.4. Anti-tumor efficacy in vivo

To further evaluate the tumor suppressive effect of the hydrogel chemo-photothermal synergistic tumor treatment in vivo, we treated tumor-bearing mice for 12 days. The treatment process is shown in Fig. 5a and mice were randomly divided into seven groups: I: PBS, II: PBS + Laser, III: DOX, IV: HS/HT@PPF hydrogel, V: HS/HT@PPF/D hydrogel, VI: HS/HT@PPF hydrogel + Laser and VII: HS/HT@PPF/D hydrogel + Laser. After the tumor volume increased to about 100 mm^3, the hydrogel was locally injected into the tumor site, and the mice were treated with different treatments for 12 days, and the tumor status in each mouse was observed (Fig. S12). The infrared thermal imaging camera recorded the temperature changes of the tumor site irradiated by the 808 nm laser in real time (Fig. 5b). After 5 min of laser irradiation in mice injected with PBS, the temperature of the tumor area only increased by 6.2 °C, which did not cause damage to the tumor. However, after injection of the hydrogel and NIR laser irradiation, the temperature of the mice tumor area increased significantly by about 28 °C (Fig. S13). This finding suggested that the HS/HT@PPF/D hydrogel

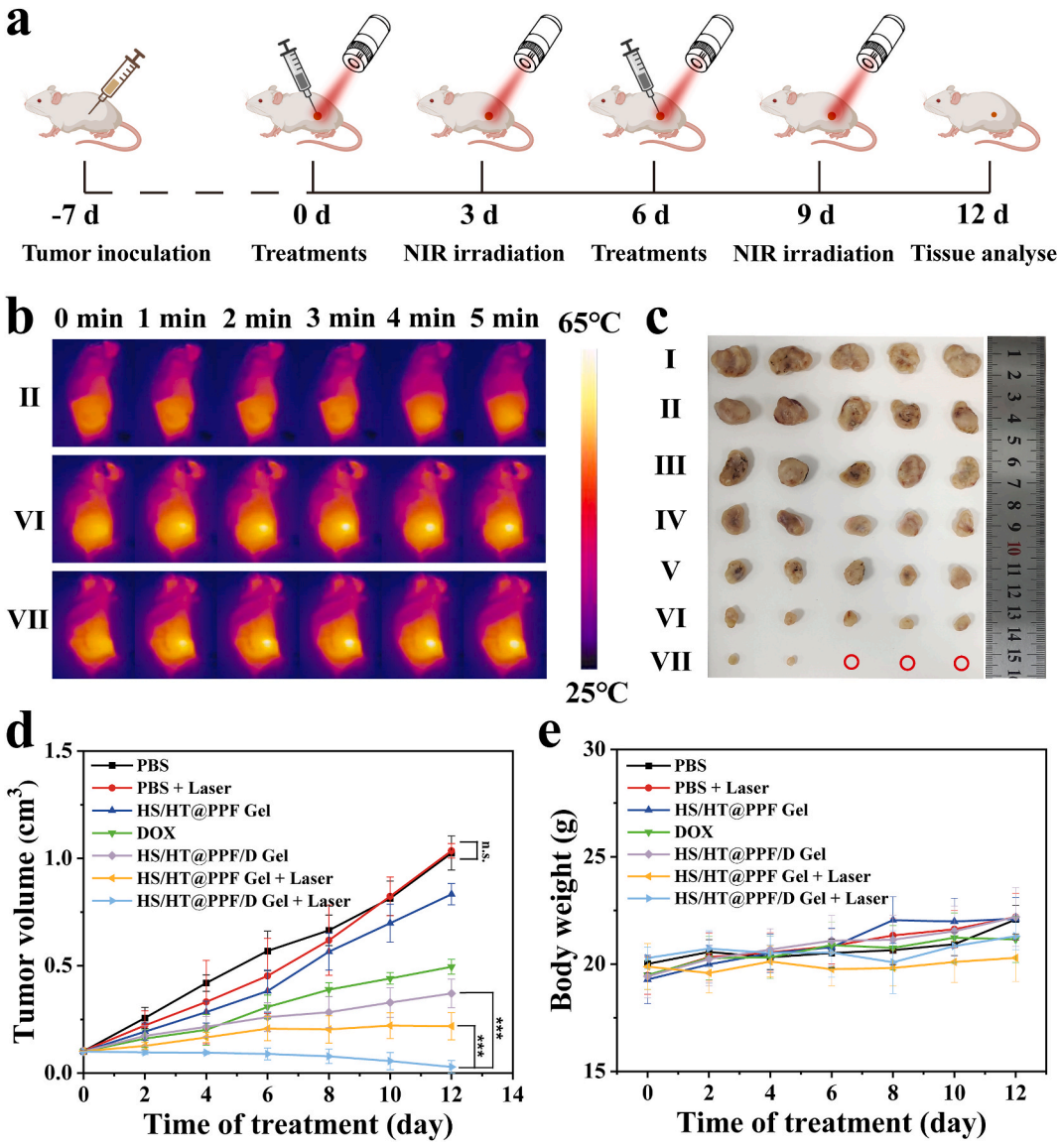

Fig. 5. (a) Time schedule of the treatment process. (b) Photothermal imaging at different time points of mice with 808 nm laser (1.0 W cm^{-2}). (c) Tumor images of seven groups after therapy (I: PBS, II: PBS + Laser, III: HS/HT@PPF hydrogel, IV: DOX, V: HS/HT@PPF/D hydrogel, VI: HS/HT@PPF hydrogel + Laser, VII: HS/HT@PPF/D hydrogel + Laser). (d) Tumor volume change during therapy. (e) Body weight changes of mice during therapy. (One-way ANOVA, n = 5, n.s., no significance, ***p < 0.001).

efficiently converts NIR light into heat above 50 °C, potentially leading to effective tumor cell ablation. Tumor volumes were monitored and recorded every two days throughout the treatment period for all groups. We found that starting from the day of administration, the tumor volume in the PBS + Laser group was similar to that of the PBS group and continued to grow, indicating that laser irradiation alone had no anti-tumor effect. DOX, HS/HT@PPF hydrogel, HS/HT@PPF/D hydrogel and HS/HT@PPF hydrogel + Laser treatment groups all showed certain anti-tumor ability, but the tumor suppressor effect was limited and the ideal therapeutic effect was not yet achieved. The tumor growth rate of the HS/HT@PPF/D hydrogel group under NIR laser irradiation was significantly lower than that of other groups, and the final tumor volume was the smallest after 12 days (Fig. 5c–d), proving that the combination of anti-tumor drugs and NIR laser irradiation effectively inhibited tumor growth. The above results indicated that the excellent synergistic therapeutic effect of chemotherapy and photothermal therapy of the hydrogel loaded with DOX and PPF. Notably, no significant body weight changes were observed across treatment groups throughout the experiment (Fig. 5e), suggesting good biocompatibility of the treatment approach.

After 12 days of treatment, the anti-tumor effect was evaluated by pathological sections and H&E staining. The results of H&E staining and TUNEL staining of tumors showed that there were almost no histological changes in PBS, PBS + Laser and HS/HT@PPF hydrogel treatment groups. The fluorescence intensity of tumor cells necrosis and apoptosis increased in the DOX, HS/HT@PPF/D hydrogel group and HS/HT@PPF hydrogel + Laser group in contrast to the control group. Moreover, tumor cells in the HS/HT@PPF/D hydrogel + Laser group showed extensive and significant necrosis, which was further confirmed by TUNEL staining (Fig. 6a). These results indicated that the hydrogel loaded with DOX and PPF had significant advantages in chemotherapy and photothermal treatment of tumors. To further evaluate the biocompatibility of the hydrogel in vivo, H&E staining was used to study the major organs of mice after 12 days of treatment (Fig. 6b). Histological staining of the treated heart, liver, spleen, lung, and kidney showed no damage or necrosis, indicating that the prepared hydrogel had high biological safety in vivo.

4. Conclusion

In summary, we successfully prepared and characterized an in situ injectable multi-stimulus-responsive HS/HT@PPF/D hydrogel, which was loaded with DOX and PPF via HRP enzymatic cross-linking reaction. This system could effectively achieve chemo-photothermal synergistic therapy of tumors. The HS/HT@PPF/D hydrogel was injectable and could quickly cross-linked in situ at the tumor site to form a porous network structure within a few minutes. The hydrogel delivery of drug could be control by multi-

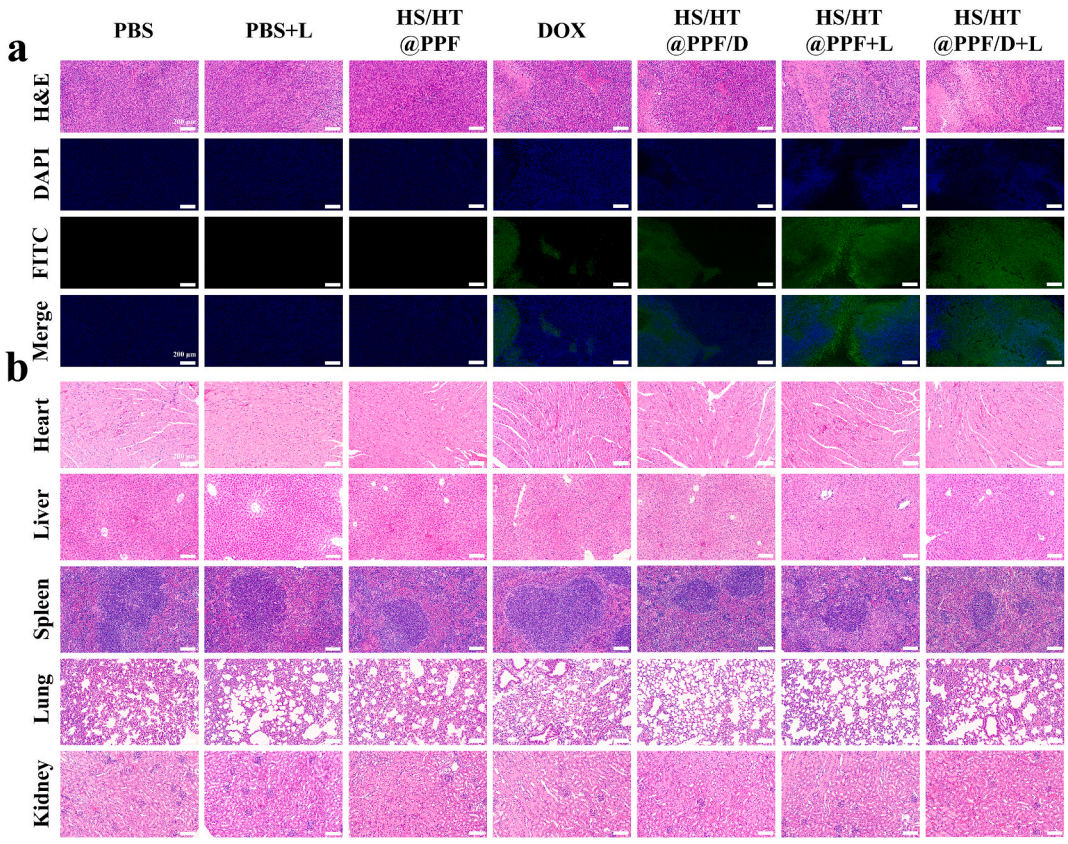

Fig. 6. (A) H&E staining and TUNEL staining images of tumor slices after different treatments. (b) Staining diagram of pathological sections of the hearts, livers, spleens, lungs and kidneys.

triggers under endogenous (weakly acidic, overexpressed GSH and HAase) and exogenous (laser) conditions, thereby performing efficient, specific and precise chemotherapy for tumors. Furthermore, the encapsulation of PPF nanoparticles with excellent targeting ability enhanced HS/HT@PPF/D hydrogel excellent photothermal property, which could effectively generate sufficient heat to kill tumor cells for photothermal therapy.

In vitro and in vivo experimental results showed that the HS/HT@PPF/D hydrogel combined with NIR laser irradiation significantly inhibit tumor proliferation. In addition, HS/HT@PPF/D with laser almost completely inhibited the growth of tumor cells, that exhibited excellent chemo-photothermal synergistic treatment effects. Moreover, the HS/HT@PPF/D hydrogel was proven to be degradable in vivo, accompanied by excellent biocompatibility. Therefore, the HS/HT@PPF/D hydrogel is a promising drug delivery platform with multi-stimulus response properties, which can be injected in situ at the tumor site to form a hydrogel for precision chemo-photothermal synergistic treatment. The drug delivery system of hydrogel is highly malleable and could be incorporated more therapeutic factors, such as mechanical factors and immune factors. This may provide new ideas for developing drug delivery systems for local synergistic tumor treatment to eliminate tumor.

CRediT authorship contribution statement

Sisi Fan: Writing – original draft, Data curation. **Qinghuan Liu:** Investigation, Data curation. **Jia Dong:** Software, Investigation. **Xiaorui Ai:** Investigation, Formal analysis, Data curation. **Jing Li:** Project administration. **Wei Huang:** Project administration, Investigation, Data curation. **Taolei Sun:** Supervision, Project administration, Funding acquisition.

Declaration of competing interest

The authors declare that they have no known competing financial interests or personal relationships that could have appeared to influence the work reported in this paper.

Acknowledgments

The work was supported by the National Natural Science Foundation of China (21703163, 52372271, 81803515) and the Fundamental Research Funds for the Central Universities (2021IVA004).

Appendix A. Supplementary data

Supplementary data to this article can be found online at https://doi.org/10.1016/j.heliyon.2024.e32135.

References

[1] H. Sung, J. Ferlay, R.L. Siegel, M. Laversanne, I. Soerjomataram, A. Jemal, F. Bray, Global cancer statistics 2020: GLOBOCAN estimates of incidence and mortality worldwide for 36 cancers in 185 countries, CA A Cancer J. Clin. 71 (2021) 209–249, https://doi.org/10.3322/caac.21660.

[2] F. Wang, H. Su, R. Lin, R.W. Chakroun, M.K. Monroe, Z. Wang, M. Porter, H. Cui, Supramolecular tubustecan hydrogel as chemotherapeutic carrier to improve tumor penetration and local treatment efficacy, ACS Nano 14 (2020) 10083–10094, https://doi.org/10.1021/acsnano.0c03286.

[3] C. Bastiancich, A. Malfanti, V. Préat, R. Rahman, Rationally designed drug delivery systems for the local treatment of resected glioblastoma, Adv. Drug Deliv. Rev. 177 (2021) 113951, https://doi.org/10.1016/j.addr.2021.113951.

[4] M. Zhou, Q. Zuo, Y. Huang, L. Li, Immunogenic hydrogel toolkit disturbing residual tumor “seeds” and pre-metastatic “soil” for inhibition of postoperative tumor recurrence and metastasis, Acta Pharm. Sin. B 12 (2022) 3383–3397, https://doi.org/10.1016/j.apsb.2022.02.017.

[5] L. Zhou, C. Dai, L. Fan, Y. Jiang, C. Liu, Z. Zhou, P. Guan, Y. Tian, J. Xing, X. Li, Y. Luo, P. Yu, C. Ning, G. Tan, Injectable self-healing natural biopolymer-based hydrogel adhesive with thermoresponsive reversible adhesion for minimally invasive surgery, Adv. Funct. Mater. 31 (2021) 2007457, https://doi.org/10.1002/adfm.202007457.

[6] C.C. Parkins, J.H. McAbee, L. Ruff, A. Wendler, R. Mair, R.J. Gilbertson, C. Watts, O.A. Scherman, Mechanically matching the rheological properties of brain tissue for drug-delivery in human glioblastoma models, Biomaterials 276 (2021) 120919, https://doi.org/10.1016/j.biomaterials.2021.120919.

[7] P. Jin, M. Xia, M. Hasany, P. Feng, J. Bai, J. Gao, W. Zhang, M. Mehrali, R. Wang, A tough injectable self-setting cement-based hydrogel for noninvasive bone augmentation, Interdisciplinary Materials 2 (2023) 771–788, https://doi.org/10.1002/idm2.12119.

[8] Q. Li, X. Li, E. Bury, K. Lackey, A. Koh, U. Wesselmann, T. Yaksh, C. Zhao, Hydration-induced void-containing hydrogels for encapsulation and sustained release of small hydrophilic molecules, Adv. Funct. Mater. 33 (2023) 2301025, https://doi.org/10.1002/adfm.202301025.

[9] X. Zhao, Y. Yang, J. Yu, R. Ding, D. Pei, Y. Zhang, G. He, Y. Cheng, A. Li, Injectable hydrogels with high drug loading through B-N coordination and ROS-triggered drug release for efficient treatment of chronic periodontitis in diabetic rats, Biomaterials 282 (2022) 121387, https://doi.org/10.1016/j.biomaterials.2022.121387.

[10] D.K. Patel, E. Jung, S. Priya, S.Y. Won, S.S. Han, Recent advances in biopolymer-based hydrogels and their potential biomedical applications, Carbohydr. Polym. 323 (2024) 121408, https://doi.org/10.1016/j.carbpol.2023.121408.

[11] W. Han, F. Liu, Y. Li, G. Liu, H. Li, Y. Xu, S. Sun, Advances in natural polymer-based transdermal drug delivery systems for tumor therapy, Small 19 (2023) 2301670, https://doi.org/10.1002/smll.202301670.

[12] J. Li, Y. Li, C. Guo, X. Wu, Development of quercetin loaded silk fibroin/soybean protein isolate hydrogels for burn wound healing, Chem. Eng. J. 481 (2024) 148458, https://doi.org/10.1016/j.cej.2023.148458.

[13] X. Wu, X. Wang, X. Chen, X. Yang, Q. Ma, G. Xu, L. Yu, J. Ding, Injectable and thermosensitive hydrogels mediating a universal macromolecular contrast agent with radiopacity for noninvasive imaging of deep tissues, Bioact. Mater. 6 (2021) 4717–4728, https://doi.org/10.1016/j.bioactmat.2021.05.013.

[14] K. Xu, H. Yao, D. Fan, L. Zhou, S. Wei, Hyaluronic acid thiol modified injectable hydrogel: synthesis, characterization, drug release, cellular drug uptake and anticancer activity, Carbohydr. Polym. 254 (2021) 117286, https://doi.org/10.1016/j.carbpol.2020.117286.

[15] F. Xu, T. Deng, W. Li, Y. Ai, J. Wu, Y. Yang, C. He, K. Yang, L. Li, F. Dai, L. Song, A sequential sustained-release hydrogel with potent antimicrobial, anti-inflammatory, and osteogenesis-promoting properties for the treatment of periodontitis, Chem. Eng. J. 477 (2023) 147195, https://doi.org/10.1016/j.cej.2023.147195.

[16] L. Tan, R. Huang, X. Li, S. Liu, Y.M. Shen, Z. Shao, Chitosan-based core-shell nanomaterials for pH-triggered release of anticancer drug and near-infrared bioimaging, Carbohydr. Polym. 157 (2017) 325–334, https://doi.org/10.1016/j.carbpol.2016.09.092.

[17] S. Káčerová, M. Muchová, H. Doudová, L. Münster, B. Hanulíková, K. Valášková, V. Kašpárková, I. Kuřitka, P. Humpolíček, Z. Víchová, O. Vašíček, J. Vícha, Chitosan/dialdehyde cellulose hydrogels with covalently anchored polypyrrole: novel conductive, antibacterial, antioxidant, immunomodulatory, and anti-inflammatory materials, Carbohydr. Polym. 327 (2024) 121640, https://doi.org/10.1016/j.carbpol.2023.121640.

[18] J.Y. Lai, L.J. Luo, D.D. Nguyen, Multifunctional glutathione-dependent hydrogel eye drops with enhanced drug bioavailability for glaucoma therapy, Chem. Eng. J. 402 (2020) 126190, https://doi.org/10.1016/j.cej.2020.126190.

[19] Z. Chen, M. Ezzo, B. Zondag, F. Rakhshani, Y. Ma, B. Hinz, E. Kumacheva, Intrafibrillar crosslinking enables decoupling of mechanical properties and structure of a composite fibrous hydrogel, Adv. Mater. 36 (2024) 2305964, https://doi.org/10.1002/adma.202305964.

[20] L. Xie, M. Shen, Y. Hong, H. Ye, L. Huang, J. Xie, Chemical modifications of polysaccharide and their anti-tumor activities, Carbohydr. Polym. 229 (2020) 115436, https://doi.org/10.1016/j.carbpol.2019.115436.

[21] F. Rizzo, N.S. Kehr, Recent advances in injectable hydrogels for controlled and local drug delivery, Adv. Healthcare Mater. 10 (2021) 2001341, https://doi.org/10.1002/adhm.202001341.

[22] J.Q. Zhu, H. Wu, Z.L. Li, X.F. Xu, H. Xing, M.D. Wang, H.D. Jia, L. Liang, C. Li, L.Y. Sun, Y.G. Wang, F. Shen, D.S. Huang, T. Yang, Responsive hydrogels based on triggered click reactions for liver cancer, Adv. Mater. 34 (2022) 2201651, https://doi.org/10.1002/adma.202201651.

[23] R. Lv, X. Li, S. Song, H. Wang, S. Gao, S. Zhang, Y. An, H. Zhou, Y. Ji, Z. Xu, Fabrication and characterization of dual-responsive nanocarriers for effective drug delivery and synergistic chem-photothermal effects, Colloids Surf. A Physicochem. Eng. Asp. 655 (2022) 130256, https://doi.org/10.1016/j.colsurfa.2022.130256.

[24] Y.J. Jo, M. Gulfam, S.H. Jo, Y.S. Gal, C.W. Oh, S.H. Park, K.T. Lim, Multi-stimuli responsive hydrogels derived from hyaluronic acid for cancer therapy application, Carbohydr. Polym. 286 (2022) 119303, https://doi.org/10.1016/j.carbpol.2022.119303.

[25] S. Song, X. Li, Y. Ji, R. Lv, L. Wu, H. Wang, M. Cao, Z. Xu, GSH/pH dual-responsive and HA-targeting nano-carriers for effective drug delivery and controlled release, J. Drug Deliv. Sci. Technol. 62 (2021) 102327, https://doi.org/10.1016/j.jddst.2021.102327.

[26] C.H. Lu, Y.C. Yeh, Fabrication of multiresponsive magnetic nanocomposite double-network hydrogels for controlled release applications, Small 17 (2021) 2105997, https://doi.org/10.1002/smll.202105997.

[27] T. Guo, W. Wang, J. Song, Y. Jin, H. Xiao, Dual-responsive carboxymethyl cellulose/dopamine/cystamine hydrogels driven by dynamic metal-ligand and redox linkages for controllable release of agrochemical, Carbohydr. Polym. 253 (2021) 117188, https://doi.org/10.1016/j.carbpol.2020.117188.

[28] K. Li, W. Dong, L. Qiu, Q. Liu, G. Lv, Y. Peng, M. Xie, J. Lin, A new GSH-responsive prodrug of 5-aminolevulinic acid for photodiagnosis and photodynamic therapy of tumors, Eur. J. Med. Chem. 181 (2019) 111582, https://doi.org/10.1016/j.ejmech.2019.111582.

[29] L. Shi, H. Lv, C. Chen, F. Cui, L. Zhang, J. Cao, R. Proietti Zaccaria, Q. Zhang, D. Sun, Regulation of gut microbiome with redox responsible bacterial cellulose hydrogel for precision chemo-radiotherapy of intestinal cancer, Chem. Eng. J. 446 (2022) 137340, https://doi.org/10.1016/j.cej.2022.137340.

[30] S. Gao, R. Lv, N. Hao, H. Wang, Y. Lv, Y. Li, Y. Ji, Y. Liu, Fabrication of pH/photothermal-responsive ZIF-8 nanocarriers loaded with baicalein for effective drug delivery and synergistic chem-photothermal effects, Colloids Surf. A Physicochem. Eng. Asp. 668 (2023) 131401, https://doi.org/10.1016/j.colsurfa.2023.131401.

[31] D. Wu, X. Shi, F. Zhao, S.T.F. Chilengue, L. Deng, A. Dong, D. Kong, W. Wang, J. Zhang, An injectable and tumor-specific responsive hydrogel with tissue-adhesive and nanomedicine-releasing abilities for precise locoregional chemotherapy, Acta Biomater. 96 (2019) 123–136, https://doi.org/10.1016/j.actbio.2019.06.033.

[32] R. Lv, H. Wang, Y. Ji, S. Gao, N. Hao, S. Zhang, Y. Lv, Q. Zhang, X. Han, Y. Liu, Z. Xu, Co-Delivery of Curcumin and doxorubicin using a pH-photothermal dual-responsive and CD44-targeted nanocarrier for enhanced chemo-photothermal synergistic tumor treatment, ChemNanoMat 10 (2024) 202300353, https://doi.org/10.1002/cnma.202300353.

[33] Z. Sun, C. Song, C. Wang, Y. Hu, J. W, Hydrogel-based controlled drug delivery for cancer treatment: a review, Mol. Pharm. 17 (2020) 373–391, https://doi.org/10.1021/acs.molpharmaceut.9b01020.

[34] H. Liu, X. Shi, D. Wu, F. Kahsay Khshen, L. Deng, A. Dong, W. Wang, J. Zhang, Injectable, biodegradable, thermosensitive nanoparticles-aggregated hydrogel with tumor-specific targeting, penetration, and release for efficient postsurgical prevention of tumor recurrence, ACS Appl. Mater. Interfaces 11 (2019) 19700–19711, https://doi.org/10.1021/acsami.9b01987.

[35] J. Lu, Y. Mao, S. Feng, X. Li, Y. Gao, Q. Zhao, S. Wang, Biomimetic smart mesoporous carbon nanozyme as a dual-GSH depletion agent and O_2 generator for enhanced photodynamic therapy, Acta Biomater. 148 (2022) 310–322, https://doi.org/10.1016/j.actbio.2022.06.001.

[36] X. Xu, Z. Zeng, Z. Huang, Y. Sun, Y. Huang, J. Chen, J. Ye, H. Yang, C. Yang, C. Zhao, Near-infrared light-triggered degradable hyaluronic acid hydrogel for on-demand drug release and combined chemo-photodynamic therapy, Carbohydr. Polym. 229 (2020) 115394, https://doi.org/10.1016/j.carbpol.2019.115394.

[37] A. Yang, X. Dong, Y. Bai, S. Sheng, Y. Zhang, T. Liu, D. Zhu, F. Lv, Doxorubicin/CpG self-assembled nanoparticles prodrug and dendritic cells co-laden hydrogel for cancer chemo-assisted immunotherapy, Chem. Eng. J. 416 (2021) 129192, https://doi.org/10.1016/j.cej.2021.129192.

[38] Q. Zhao, Y. Zhang, T. Yu, J. Lu, G. Sun, X. Luo, S. Wang, Tailored nanoplatforms with detachable 'meteorolite' for photothermal-enhanced programmed tumor therapy, Carbon 199 (2022) 119–131, https://doi.org/10.1016/j.carbon.2022.07.073.

[39] K. Yang, S. Zhao, B. Li, B. Wang, M. Lan, X. Song, Low temperature photothermal therapy: advances and perspectives, Coord. Chem. Rev. 454 (2022) 214330, https://doi.org/10.1016/j.ccr.2021.214330.

[40] X. Wang, J. Dai, C. Shao, T. Goto, H. Dai, Emerging advances in fluorescence imaging and phototherapy of arthritis, Interdisciplinary Materials 2 (2023) 803–832, https://doi.org/10.1002/idm2.12130.

[41] H. Xu, Y. Zhang, H. Zhang, Y. Zhang, Q. Xu, J. Lu, S. Feng, X. Luo, S. Wang, Q. Zhao, Smart polydopamine-based nanoplatforms for biomedical applications: state-of-art and further perspectives, Coord. Chem. Rev. 488 (2023) 215153, https://doi.org/10.1016/j.ccr.2023.215153.

[42] J. Lu, L. Song, S. Feng, K. Wang, Y. Mao, Y. Gao, Q. Zhao, S. Wang, Nanozyme-mediated biocatalysis as a mitochondrial oxidative stress amplifier for tumor nanocatalytic immunotherapy, Chem. Eng. J. 481 (2024) 148270, https://doi.org/10.1016/j.cej.2023.148270.

[43] S. Su, Y. Ding, Y. Li, Y. Wu, G. Nie, Integration of photothermal therapy and synergistic chemotherapy by a porphyrin self-assembled micelle confers chemosensitivity in triple-negative breast cancer, Biomaterials 80 (2016) 169–178, https://doi.org/10.1016/j.biomaterials.2015.11.058.

[44] G. Wei, G. Yang, B. Wei, Y. Wang, S. Zhou, Near-infrared light switching nitric oxide nanoemitter for triple-combination therapy of multidrug resistant cancer, Acta Biomater. 100 (2019) 365–377, https://doi.org/10.1016/j.actbio.2019.10.002.

[45] A. Jin, Y. Wang, K. Lin, L. Jiang, Nanoparticles modified by polydopamine: working as "drug" carriers, Bioact. Mater. 5 (2020) 522–541, https://doi.org/10.1016/j.bioactmat.2020.04.003.

[46] Z. Zhang, J. Zhang, J. Tian, H. Li, A polydopamine nanomedicine used in photothermal therapy for liver cancer knocks down the anti-cancer target NEDD8-E3 ligase ROC1 (RBX1), J. Nanobiotechnol. 19 (2021) 323, https://doi.org/10.1186/s12951-021-01063-4.

[47] M. Khanmohammadi, M.B. Dastjerdi, A. Ai, A. Ahmadi, A. Godarzi, A. Rahimi, J. Ai, Horseradish peroxidase-catalyzed hydrogelation for biomedical applications, Biomater. Sci. 6 (2018) 1286–1298, https://doi.org/10.1039/C8BM00056E.

[48] T.T. Hoang Thi, Y. Lee, S.B. Ryu, D.H. Nguyen, K.D. Park, Enhanced tissue adhesiveness of injectable gelatin hydrogels through dual catalytic activity of horseradish peroxidase, Biopolymers 109 (2018) 23077, https://doi.org/10.1002/bip.23077.

[49] Y. Liu, K. Ai, J. Liu, M. Deng, Y. He, L. Lu, Dopamine-melanin colloidal nanospheres: an efficient near-infrared photothermal therapeutic agent for in vivo cancer therapy, Adv. Mater. 25 (2013) 1353–1359, https://doi.org/10.1002/adma.201204683.